Original Article

Simultaneous multislice echo-planar diffusion-weighted imaging (DWI) in patients with focal liver lesions: a comparative study with conventional DWI

Yingyi Wu[1#^], Zheng Ye[1#^], Ting Yang[1^], Shan Yao[1^], Jie Chen[1^], Ting Yin[2^], Hehan Tang[1*^], Bin Song[1,3*^]

[1]Department of Radiology, West China Hospital, Sichuan University, Chengdu, China; [2]MR Collaborations, Siemens Healthineers Ltd., Chengdu, China; [3]Department of Radiology, Sanya People's Hospital, Sanya, China

Contributions: (I) Conception and design: Z Ye, Y Wu; (II) Administrative support: H Tang, B Song; (III) Funding acquisition: Z Ye, B Song; (IV) Provision of study materials or patients: Z Ye, Y Wu; (V) Collection and assembly of data: Y Wu, Z Ye, T Yang, S Yao; (VI) Data analysis and interpretation: Y Wu, Z Ye, J Chen; (VII) Manuscript writing: All authors; (VIII) Final approval of manuscript: All authors.

[#]These authors contributed equally to this work.

[*]These authors contributed equally to this work as senior authors.

Correspondence to: Hehan Tang, MD. Department of Radiology, West China Hospital, Sichuan University, No. 37 Guoxue Alley, Chengdu 610041, China. Email: lanny.320@163.com; Bin Song, MD, PhD. Department of Radiology, West China Hospital, Sichuan University, No. 37 Guoxue Alley, Chengdu 610041, China; Department of Radiology, Sanya People's Hospital, Sanya, China. Email: songlab_radiology@163.com.

Background: Simultaneous multislice (SMS) technology improves acquisition efficiency of diffusion-weighted imaging (DWI). This study aimed to evaluate the performance of SMS-DWI in image quality and apparent diffusion coefficient (ADC) measurements for focal liver lesions (FLLs) as compared with that of conventional DWI (CON-DWI).

Methods: The institutional ethics committee of West China Hospital, Sichuan University approved this single-center, prospective study conducted from February 2021 to March 2022. Free-breathing SMS-DWI and CON-DWI examinations were acquired on a 3-T scanner with b-values of 50, 400, and 800 s/mm^2. Qualitative image quality and quantitative measurements of signal-to-noise ratio (SNR), contrast-to-noise ratio (CNR), and ADC were compared between SMS-DWI and CON-DWI. The ADC values for FLLs were further compared between SMS-DWI and CON-DWI in different patient subgroups. The intra- and interreader agreements were assessed. Significance was set at $P<0.05$.

Results: This study included 116 patients (96 males, 20 females; mean age 52.0±10.7 years) with 119 FLLs. No significant differences were observed between SMS-DWI and CON-DWI regarding overall image quality in any b-value DWIs, and there were also no differences observed between SMS-DWI and CON-DWI (b=800 s/mm^2) for either SNR or CNR (both P values >0.05). ADC values obtained from CON-DWI were higher than those from SMS-DWI in all FLLs [$(1.31\pm0.47)\times10^{-3}$ *vs.* $(1.26\pm0.46)\times10^{-3}$ mm^2/s; P=0.004], and similar findings were observed across the different patient subgroups. The consistency analysis showed intrareader intraclass correlation coefficient (ICC) values of 0.792–0.944 and interreader ICC values of

^ ORCID: Yingyi Wu, 0000-0002-6499-3211; Zheng Ye, 0000-0001-6715-0183; Ting Yang, 0000-0002-5651-5324; Shan Yao, 0000-0002-0665-2566; Jie Chen, 0000-0001-7446-7541; Ting Yin, 0000-0003-2528-1630; Hehan Tang, 0000-0002-3882-4270; Bin Song, 0000-0002-7269-2101.

0.758–0.861 for quantitative measurements (SNR, CNR, and ADC) and kappa values of 0.609–0.878 for qualitative image quality.

Conclusions: SMS-DWI achieved a 37% reduction in scan time compared to CON-DWI while maintaining comparable overall image quality. Notably, the ADC values for FLLs were observed to be quantitatively lower with SMS-DWI.

Keywords: Liver; magnetic resonance imaging (MRI); simultaneous multislice (SMS); diffusion-weighted imaging (DWI); apparent diffusion coefficient (ADC)

Submitted Feb 22, 2024. Accepted for publication Aug 08, 2024. Published online Aug 28, 2024.
doi: 10.21037/qims-24-341
View this article at: https://dx.doi.org/10.21037/qims-24-341

Introduction

Accurate characterization of focal liver lesions (FLLs) is essential for appropriate patient management. Benign FLLs, such as cysts and hemangiomas, usually require need regular follow-up, while malignant liver tumors necessitate treatment, such as surgical resection or liver transplantation (1). Magnetic resonance imaging (MRI) has been widely applied in the differential diagnosis of FLLs (2,3), and diffusion-weighted imaging (DWI) is one of the most useful tools in this regard (4-9).

The DWI technique is based on the random Brownian motion of water molecules within the tissues, and it can reflect the degree of restricted diffusion of biological tissues (10). The quantitative apparent diffusion coefficient (ADC), typically derived using a monoexponential model from DWI, offers important diffusional information and serves as a valuable imaging biomarker. For instance, ADC can be used for the differentiation of benign and malignant FLLs (5), the detection and monitoring of liver metastases (11), and the prediction of liver tumor aggressiveness and patient prognosis (4).

Despite its advantages, the single-shot conventional DWI (CON-DWI) still encounters certain problems in liver imaging (12), for example, a reduced signal-to-noise ratio (SNR) when the breath-hold technique in DWI is being employed and a relatively lengthy acquisition times associated with triggered DWI techniques. The long acquisition duration can lead to patient discomfort and hinder efficient clinical workflow. Moreover, artifacts such as respiratory motion can degrade the image quality by blurring. Simultaneous multislice (SMS) imaging is a technique that allows scanning with reduced duration via simultaneous excitation and acquisition of multiple slices (13). Typically, SMS-DWI uses a multiband radio frequency (RF) excitation and echo-planar imaging (EPI) readout in combination with the blipped controlled aliasing in parallel imaging resulting in higher acceleration (CAIPIRINHA) technique (14,15). SMS-DWI has been proven feasible, has a significantly shortened scan duration, and has shown great promise in the imaging of the liver (16), pancreas (17), prostate (18), rectum (19), and kidney (20).

Previous studies have demonstrated that SMS-DWI with an acceleration factor of 2 can significantly reduce the scan time while maintaining a similar SNR and image quality (21). However, the effect of the SMS technique on quantitative parameters of abdominal DWI remains controversial. Some studies have reported no significant difference in liver ADC values between SMS-DWI and CON-DWI (22,23). Meanwhile, others have indicated that SMS-DWI yields lower or higher ADC values in abdominal organs than does CON-DWI (16,21,24,25). Moreover, previous research in this area has mainly focused on validating the feasibility of SMS-DWI in abdominal imaging, often with limited sample sizes (16,21,22,26). Therefore, the application of SMS-DWI for patients with FLLs remains to be clarified by more intensive investigation.

Therefore, this prospective study aimed to evaluate the performance of SMS-DWI in image quality [including SNR and contrast-to-noise ratio (CNR) measurements] and ADC measurements as compared with that of the clinical standard CON-DWI. We present this article in accordance with the GRRAS reporting checklist (available at https://qims.amegroups.com/article/view/10.21037/qims-24-341/rc).

Methods

Patient selection

This prospective study was approved by the ethics

Table 1 The detailed acquisition parameters of SMS-DWI and CON-DWI

Parameter	SMS-DWI	CON-DWI
Image acquisition technique	Free-breathing	Free-breathing
Repetition time (ms)	2,000	3,200
Echo time (ms)	63	63
Echo spacing (ms)	0.5	0.5
Field of view (mm^2)	400×288	400×288
Scan matrix	128×94	128×94
Slice thickness (mm)	5	5
Slice gap (mm)	1.5	1.5
No. of slices	22	22
Bandwidth (Hz/pixel)	2,442	2,442
b-value (s/mm^2)	50, 400, 800	50, 400, 800
No. of signals acquired	1, 2, 4	1, 2, 4
Diffusion mode	3-Scan Trace	3-Scan Trace
Diffusion scheme	Monopolar	Monopolar
Parallel acceleration	GRAPPA 2	GRAPPA 2
SMS acceleration factor	2	–
Fat saturation*	Fat sat	Fat sat
Acquisition time (s)	52	83

*, fat saturation was performed with the chemical shift method. SMS, simultaneous multislice; DWI, diffusion-weighted imaging; CON, conventional; GRAPPA, generalized autocalibrating partial parallel acquisition.

committee of West China Hospital, Sichuan University (No. 2021[107]) and was conducted in accordance with the Declaration of Helsinki (as revised in 2013). Informed consent was obtained from 336 consecutive patients between February 2021 and March 2022. The inclusion criteria for patients were (I) an age ≥18 years and (II) a clinical history, previous radiological exams, or laboratory tests suggesting FLLs. Meanwhile, the exclusion criteria were as follows: (I) contraindications to MRI examinations; (II) the absence of definite lesion; (III) nonprimary lesions; and (IV) an unclear diagnosis. All malignant and some benign FLLs were confirmed histopathologically, while the remaining benign FLLs were identified through radiological examinations, serological tumor markers, and clinical follow-up.

MRI protocol

All MRI scans were performed on a 3-T MRI scanner (MAGNETOM Skyra, Siemens Healthineers, Erlangen, Germany) equipped with an 18-channel phased-array coil for abdominal and spine imaging. Patients were instructed to fast for 4 to 6 hours before the examination. In addition to routine clinical T_1-weighted imaging (T_1WI) and T_2-weighted imaging (T_2WI) for localization, free-breathing SMS-DWI and CON-DWI sequences were acquired with b-values of 50, 400, and 800 s/mm^2, and the SMS acceleration factor was 2. The acquisition time for SMS-DWI and CON-DWI was 52 and 83 seconds, respectively. The corresponding ADC maps were generated using the monoexponential fitting algorithm (27). The detailed scanning parameters are summarized in *Table 1*.

Image analysis

Qualitative and quantitative evaluations were independently performed by two radiologists with 5 and 7 years of experience in abdominal imaging, respectively. The radiologists were blinded to the clinical information and pathological results of the patients.

Image quality assessment

DWI images (b-values of 50, 400, and 800 s/mm^2) were reviewed and rated on a 5-point Likert scale for image quality evaluation (28). The evaluation indicators included overall image quality, clarity of intrahepatic vessels, sharpness of hepatic edge, image artifact, and lesion conspicuity.

SNR and CNR measurements

The signal intensity (SI) of the lesion and liver parenchyma and the standard deviation (SD) of background noise were measured using approximately 300-pixel circular regions of interest (ROIs) on the DWI image (800 s/mm^2), as illustrated in *Figure 1*. The ROI of the lesion was positioned centrally within the tumor, with areas of hemorrhage and necrosis being avoided, while the ROI of liver parenchyma was placed in the right lobe to avoid vasculature and prominent artifacts. The ROI for background noise was positioned in the upper left corner of the image.

The SNR was calculated as the ratio of the average SI of the liver parenchyma to the SD of the background noise for

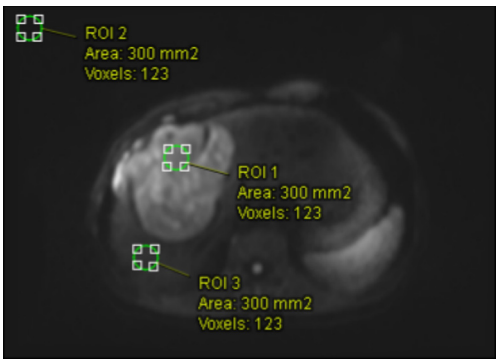

Figure 1 Measurement of SI and SD of the background noise on the diffusion-weighted image (b=800 s/mm^2). A circular ROI of approximately 300 pixels was used. The lesion ROI was placed centrally within the tumor, with areas of hemorrhage and necrosis being excluded. The liver parenchyma ROI was placed in the right lobe, with vasculature and prominent artifacts being avoided. The background noise ROI was positioned in the upper left corner of the image. ROI, region of interest; SI, signal intensity; SD, standard deviation.

DWI images with b-values of 800 s/mm^2 as follows (23,29):

$$SNR = SI_{\text{liver parenchyma}} / SD_{\text{background}} \quad [1]$$

The CNR was calculated as the absolute difference between the SI of the lesion and the SI of the liver divided by the SD of the background noise for images with b-values of 800 s/mm^2 as follows (30,31):

$$CNR = \left| SI_{\text{lesion}} - SI_{\text{liver parenchyma}} \right| / SD_{\text{background}} \quad [2]$$

ADC measurements

Quantitative ADC analysis was conducted 1 month after subjective scoring, with each radiologist independently performing two measurements. The average ADC measurements from the two radiologists were used for statistical analysis. The specific measurement steps were as follows: the slice with the maximum section of the tumor tissue on the DWI image (b=400 s/mm^2) and the slice above and below it (a total of three slices) were selected to delineate the tumor, with T_1WI and T_2WI images serving as the reference. A free-hand ROI was manually drawn along the entire tumor margin on each of the three slices, with hemorrhage, necrosis, and calcification within the tumor being avoided. The ROIs in the DWI images (b=400 s/mm^2) were then copied to the ADC maps, as illustrated in *Figure 2*. The ROIs on the axial planes of the SMS-DWI and CON-DWI sequences were kept as consistent as possible.

Statistical analysis

Descriptive statistics are presented as the mean ± SD or as the median and interquartile range depending on the data distribution. The Wilcoxon signed-rank test was used to compare the image quality between SMS-DWI and CON-DWI. For quantitative data, normality was tested with the Kolmogorov-Smirnov test and Shapiro-Wilk test, and the Wilcoxon signed-rank test or paired *t*-test was used to compare the SNR, CNR, and the ADC measurements between SMS-DWI and CON-DWI. The inter- or intrareader agreement was computed by weighted kappa coefficients or intraclass correlation coefficients (ICCs), with 0.01–0.20 representing slight agreement, 0.21–0.40 fair, 0.41–0.60 moderate, 0.61–0.80 good, and 0.81–1.00 excellent agreement (32). The comparison of ROI segmentations by two radiologists was assessed using the Dice similarity coefficient (DSC) calculated in Python (Python Software Foundation, Wilmington, DE, USA); details of the segmentation and calculation process are provided in the Appendix 1. Qualitative image quality assessment and quantitative measurements were analyzed with the MR Body Diffusion tool v. 1.4.0. The ROI segmentations were performed using ITK-SNAP v. 4.2.0) (33). Statistical analysis was performed using SPSS 25 (IBM Corp., Armonk, NY, USA) and MedCalc v. 20.1 (MedCalc Software, Ostend, Belgium) software. Differences were considered statistically significant at a bilateral P value <0.05.

Results

Patients and lesions

A total of 116 patients (96 males and 20 females; mean age 52.0±10.7 years) comprising 119 FLLs were included in this study. The basic clinical information of the included patients is summarized in *Table 2*. FLLs included hepatocellular carcinoma (n=79), intrahepatic cholangiocarcinoma (iCCA) (n=10), combined hepatocellular and cholangiocarcinoma (n=2), hemangioma (n=15), focal nodular hyperplasia (n=5), hepatic cyst (n=3), hepatocellular adenoma (HCC) (n=2), angiomyolipoma (n=1), hepatic regenerative nodule (n=1), and inflammatory myofibroblastic tumor (n=1). Representative images obtained by SMS-DWI and CON-DWI are shown in *Figures 3-6*.

Comparison of image quality

The subjective scores for SMS-DWI and CON-DWI of

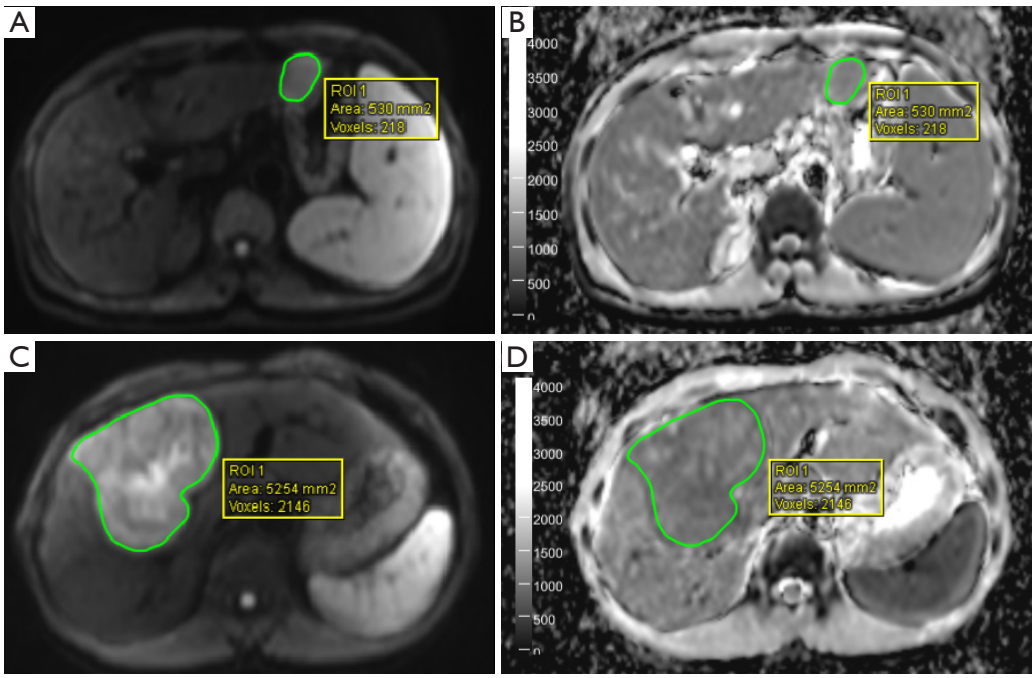

Figure 2 The illustrations of the ROI delineation process for quantitative ADC measurements of FLLs. (A,C) The diffusion-weighted images acquired at 400 s/mm^2. First, the lesion ROI is defined on the DWI image (b=400 s/mm^2) and then applied to the corresponding ADC maps (B,D). ROI, region of interest; ADC, apparent diffusion coefficient; FLL, focal liver lesion.

Table 2 Basic clinical information of the included patients

Characteristics	All patients (n=116)	Patients with malignant FLLs (n=90)	Patients with benign FLLs (n=26)
Age (years)†	52.0±10.7 [28–76]	53.4±10.6 [29–76]	46.8±10.6 [28–67]
Male/female	96/20	77/13	19/7
BMI (kg/m^2)	23.4±2.8	23.1±2.8	24.2±2.8
Etiology of liver disease			
Hepatitis B virus	72 (62.1)	67 (74.4)	5 (19.2)
Hepatitis C virus	2 (1.7)	2 (2.2)	0 (0)
Both hepatitis B & C virus	2 (1.7)	2 (2.2)	0 (0)
Others	40 (34.5)	19 (21.1)	21 (80.8)
Tumor size (cm)†*	5.50±2.7 [1.1–13.2]	5.8±2.5 [1.1–10.5]	4.3±2.8 [1.5–13.2]
Cirrhosis	46 (39.7)	41 (45.6)	5 (19.2)
BCLC stage‡			
0	–	5 (6.3)	–
A	–	57 (72.2)	–
B	–	17 (21.5)	–

†, data are expressed as the mean ± standard deviation with ranges in square brackets; *, data were calculated by the size of each lesion; ‡, BCLC stage is suitable for hepatocellular carcinoma (n=79). Unless indicated otherwise, data represent the number of patients, with percentages in parentheses. FLL, focal liver lesion; BMI, body mass index; BCLC, Barcelona Clinic Liver Cancer.

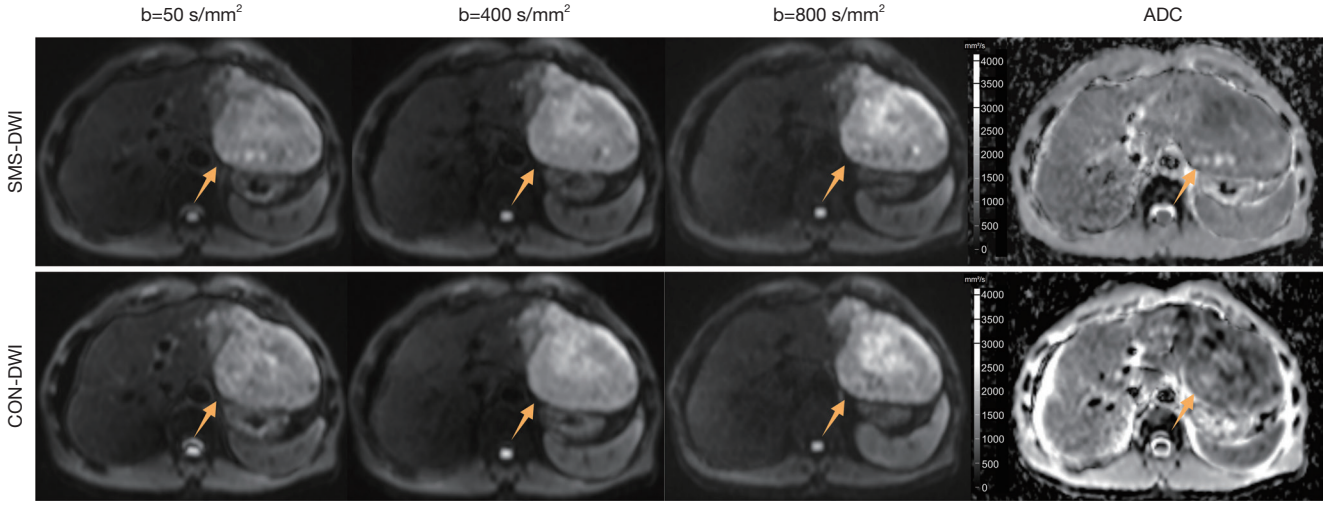

Figure 3 Representative images with SMS-DWI (upper row) and CON-DWI (lower row) of a 58-year-old male patient with pathologically confirmed hepatocellular carcinoma. Diffusion-weighted trace images with three different b-values (b=50, b=400, b=800 s/mm^2) and the corresponding ADC maps are shown, with the arrows pointing to the lesion. The average ADC measurements were 1.10×10^{-3} mm^2/s in SMS-DWI and 1.14×10^{-3} mm^2/s in CON-DWI. SMS, simultaneous multislice; DWI, diffusion-weighted imaging; ADC, apparent diffusion coefficient; CON, conventional.

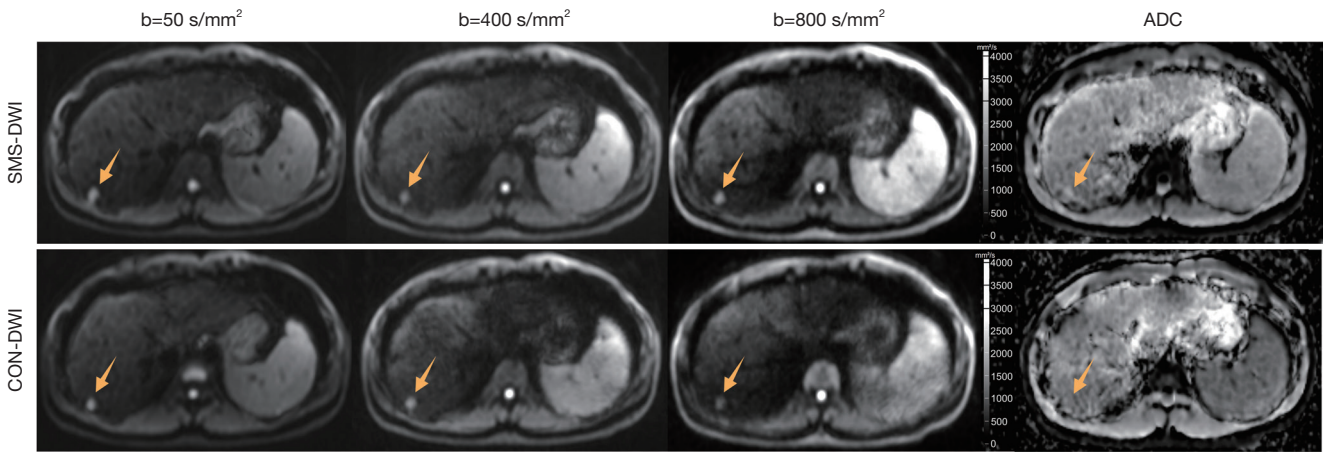

Figure 4 Representative images with SMS-DWI (upper row) and CON-DWI (lower row) of a 29-year-old male patient with pathologically confirmed hepatocellular carcinoma. Diffusion-weighted trace images with three different b-values (b=50, b=400, b=800 s/mm^2) and the corresponding ADC maps are shown, with the arrows pointing to the lesion. The average ADC measurements were 1.08×10^{-3} mm^2/s in SMS-DWI and 1.11×10^{-3} mm^2/s in CON-DWI. SMS, simultaneous multislice; DWI, diffusion-weighted imaging; ADC, apparent diffusion coefficient; CON, conventional.

each b-value are summarized in *Table 3*. No significant differences were observed between SMS-DWI and CON-DWI regarding overall image quality, sharpness of hepatic edge, and image artifact in any b-values. However, CON-DWI demonstrated significantly superior clarity of intrahepatic vessels (4.33±0.61 *vs.* 4.29±0.62; P=0.031) on b=50 s/mm^2 images. Additionally, on b=400 s/mm^2 and b=800 s/mm^2 images, SMS-DWI exhibited significantly better lesion conspicuity than did CON-DWI (b=400 s/mm^2: 4.50±0.72 *vs.* 4.47±0.73, P=0.037; b=800 s/mm^2: 4.14±0.84

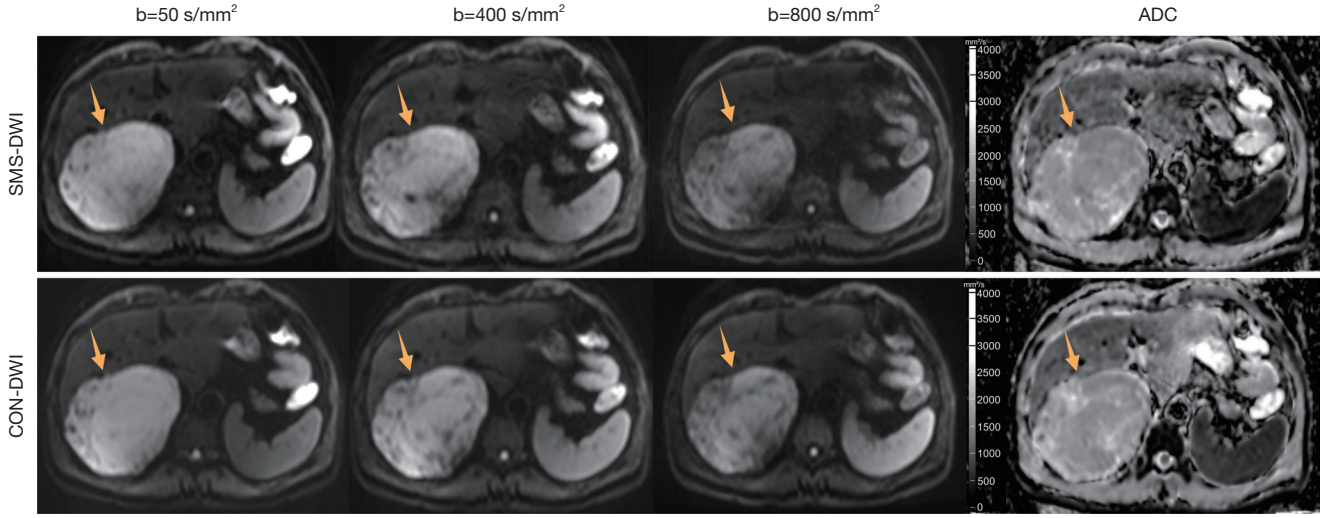

Figure 5 Representative images with SMS-DWI (upper row) and CON-DWI (lower row) of a 59-year-old male patient with pathologically confirmed hepatic cavernous hemangioma. Diffusion-weighted trace images with three different b-values (b=50, b=400, b=800 s/mm^2) and the corresponding ADC maps are shown, with the arrows pointing to the lesion. The average ADC measurements were 1.76×10^{-3} mm^2/s in SMS-DWI and 1.81×10^{-3} mm^2/s in CON-DWI. SMS, simultaneous multislice; DWI, diffusion-weighted imaging; ADC, apparent diffusion coefficient; CON, conventional.

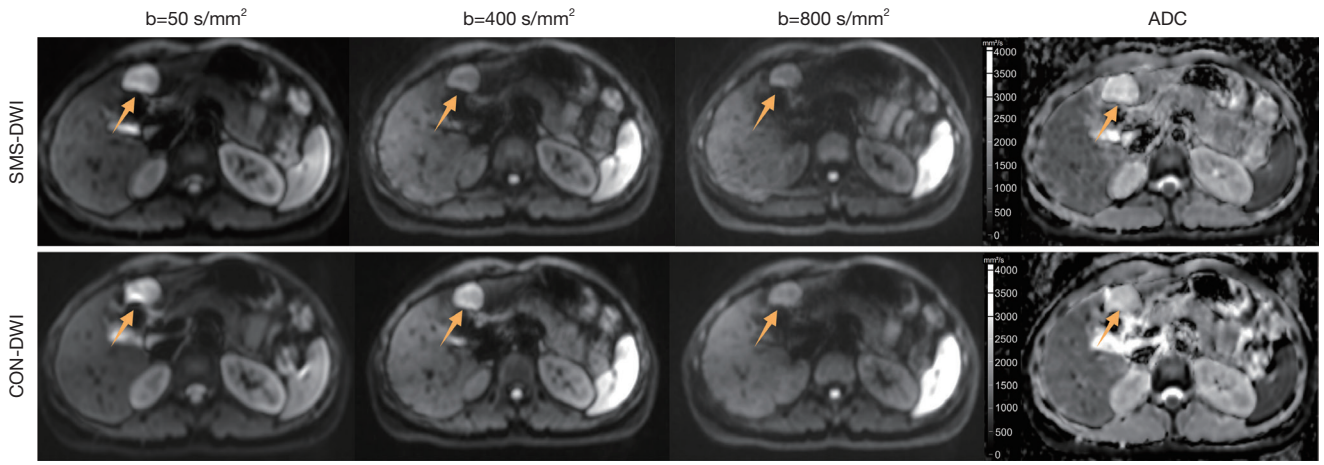

Figure 6 Representative images with SMS-DWI (upper row) and CON-DWI (lower row) of a 37-year-old female patient with hepatic cavernous hemangioma as confirmed through imaging and follow-up. Diffusion-weighted trace images with three different b-values (b=50, b=400, b=800 s/mm^2) and the corresponding ADC maps are shown, with the arrows pointing to the lesion. The average ADC measurements were 2.46×10^{-3} mm^2/s in SMS-DWI and 2.47×10^{-3} mm^2/s in CON-DWI. SMS, simultaneous multislice; DWI, diffusion-weighted imaging; ADC, apparent diffusion coefficient; CON, conventional.

vs. 4.08±0.92, P=0.013). The interreader agreement of the two radiologists was good to excellent, with kappa values ranging from 0.609 [95% confidence interval (CI): 0.479–0.782] to 0.878 (95% CI: 0.792–0.936), as presented in Table S1.

Comparison of SNR and CNR measurements

The SNR and CNR values for SMS-DWI and CON-DWI are presented in *Table 4*. There were no statistically significant differences in SNR or CNR between SMS-DWI

Table 3 Comparison of image quality between SMS-DWI and CON-DWI

Category	SMS-DWI			CON-DWI			P value
	Reader 1	Reader 2	Average	Reader 1	Reader 2	Average	
Overall image quality							
b=50 s/mm^2	4.61 [4–5]	4.56 [4–5]	4.58 [4–5]	4.60 [4–5]	4.55 [4–5]	4.58 [4–5]	0.317
b=400 s/mm^2	4.26 [4–5]	4.24 [4–5]	4.25 [4–5]	4.28 [4–5]	4.25 [4–5]	4.27 [4–5]	0.059
b=800 s/mm^2	3.85 [3–4]	3.81 [3–4]	3.82 [3–4]	3.87 [3–4]	3.84 [3–4]	3.85 [3–4]	0.058
Clarity of intrahepatic vessels							
b=50 s/mm^2	4.32 [4–5]	4.27 [4–5]	4.29 [4–5]	4.39 [4–5]	4.26 [4–5]	4.33 [4–5]	0.031*
b=400 s/mm^2	3.95 [3–4]	3.92 [3–4]	3.93 [3–4]	3.93 [3–4]	3.91 [3–4]	3.92 [3–4]	0.275
b=800 s/mm^2	3.54 [3–4]	3.50 [3–4]	3.52 [3–4]	3.55 [3–4]	3.50 [3–4]	3.53 [3–4]	0.157
Sharpness of hepatic edge							
b=50 s/mm^2	4.51 [4–5]	4.45 [4–5]	4.48 [4–5]	4.50 [4–5]	4.47 [4–5]	4.48 [4–5]	0.739
b=400 s/mm^2	4.23 [4–5]	4.12 [4–5]	4.18 [4–5]	4.27 [4–5]	4.13 [4–5]	4.20 [4–5]	0.058
b=800 s/mm^2	3.86 [3–4]	3.71 [3–4]	3.74 [3–4]	3.87 [3–4]	3.70 [3–4]	3.76 [3–4]	0.157
Artifacts							
b=50 s/mm^2	3.98 [3–4]	3.97 [3–4]	3.97 [3–4]	3.99 [3–4]	3.98 [3–4]	3.99 [3–4]	0.074
b=400 s/mm^2	3.91 [3–4]	3.88 [3–4]	3.90 [3–4]	3.93 [3–4]	3.91 [3–4]	3.92 [3–4]	0.051
b=800 s/mm^2	3.80 [3–4]	3.82 [3–4]	3.81 [3–4]	3.85 [3–4]	3.82 [3–4]	3.83 [3–4]	0.089
Lesion conspicuity							
b=50 s/mm^2	4.72 [4–5]	4.74 [4–5]	4.73 [4–5]	4.71 [4–5]	4.73 [4–5]	4.72 [4–5]	0.480
b=400 s/mm^2	4.49 [4–5]	4.50 [4–5]	4.50 [4–5]	4.46 [4–5]	4.47 [4–5]	4.47 [4–5]	0.037*
b=800 s/mm^2	4.15 [4–5]	4.12 [4–5]	4.14 [4–5]	4.09 [3–5]	4.06 [3–5]	4.08 [3–5]	0.013*

The subjective scores on a 5-point scale are presented as means [interquartile ranges], with 1 indicating the lowest quality and 5 indicating the highest quality. The P values were calculated as a comparison of the average ratings between the SMS-DWI and CON-DWI. *, statistically significant (P<0.05). SMS, simultaneous multislice; DWI, diffusion-weighted imaging; CON, conventional.

and CON-DWI on the DWI (b=800 s/mm^2). Specifically, the SNR values for SMS-DWI and CON-DWI were 140.6±58.1 and 138.5±54.6 (P=0.47), respectively, while the CNR values were 308.6±245.3 and 304.7±227.0 (P=0.33), respectively. The intra- and interreader agreement for SNR and CNR measurements between the two radiologists ranged from moderate to excellent, with ICC values from 0.758 (95% CI: 0.668–0.809) to 0.821 (95% CI: 0.805–0.851), as presented in Table S2.

Comparison of ADC measurements

The ADC measurements of SMS-DWI and CON-DWI based on the category of FLLs are presented in *Table 5*. ADC values obtained from CON-DWI were higher than those from SMS-DWI in all FLLs (P=0.004). Specifically, for HCC and iCCA, CON-DWI yielded higher ADC values than did SMS-DWI [HCC: (1.14±0.22)×10^{-3} *vs.* (1.09±0.25)×10^{-3} mm^2/s, P=0.003; iCCA: (1.14±0.22)×10^{-3} *vs.* (1.09±0.25)×10^{-3} mm^2/s, P=0.040]. Furthermore, similar findings were observed in the other types of FLLs, although the differences were not statistically significant.

The intra- and interreader agreement for quantitative ADC measurements between the two radiologists ranged from moderate to excellent, with ICC values from 0.776 (95% CI: 0.691–0.832) to 0.944 (95% CI: 0.925–0.973), as presented in Table S3. The DSC values for ROI segmentations by the radiologists on SMS-DWI and CON-

Table 4 Comparisons of SNR and CNR between SMS-DWI and CON-DWI

Parameter	SMS-DWI			CON-DWI			P value
	Reader 1	Reader 2	Average	Reader 1	Reader 2	Average	
SNR	133.5±61.2	143.9±54.5	140.6±58.1	136.1±57.3	144.4±52.2	138.5±54.6	0.47
CNR	296.5±227.8	315.0±251.4	308.6±245.3	301.6±219.7	311.9±238.5	304.7±227.0	0.33

Data are expressed as the mean ± standard deviation. The SNR and CNR were measured on DWI (b=800 mm^2/s) images. The P values were calculated as a comparison of the average SNR and CNR measurements between the SMS-DWI and CON-DWI. SNR, signal-to-noise ratio; CNR, contrast-to-noise ratio; SMS, simultaneous multislice; DWI, diffusion-weighted imaging; CON, conventional.

Table 5 Comparisons of ADC measurements for different FLL categories between SMS-DWI and CON-DWI

Lesion type	N	SMS-DWI			CON-DWI			P values
		Reader 1	Reader 2	Average	Reader 1	Reader 2	Average	
All lesions	119	1.25±0.47	1.27±0.46	1.26±0.46	1.32±0.49	1.30±0.48	1.31±0.47	0.004*
HCC	79	1.09±0.25	1.10±0.24	1.09±0.24	1.16±0.27	1.15±0.25	1.16±0.26	0.001*
iCCA	10	0.99±0.16	1.01± 0.17	1.00±0.16	1.05±0.17	1.04±0.14	1.05±0.16	0.040*
CHC	2	1.03±0.02	1.08± 0.01	1.06±0.02	1.05±0.01	1.08±0.01	1.06±0.01	–
Hemangioma	15	1.95±0.58	1.98±0.55	1.96±0.57	1.97±0.57	2.01±0.59	1.99±0.59	0.420
FNH	5	1.40±0.08	1.37±0.09	1.38±0.09	1.41±0.07	1.38±0.06	1.40±0.07	0.457
Cyst	3	2.37±0.07	2.33±0.08	2.35±0.06	2.38±0.12	2.35±0.09	2.37±0.10	0.601
Adenoma	2	1.22±0.07	1.25±0.06	1.24±0.06	1.27±0.07	1.33±0.06	1.31±0.06	–
IMT	1	1.00±0.03	0.95±0.02	0.98±0.05	1.04±0.04	1.03±0.02	1.04±0.03	–
Angiomyolipoma	1	1.11±0.02	1.08±0.02	1.10±0.03	1.20±0.04	1.22±0.04	1.21±0.04	–
RN	1	1.55±0.02	1.52±0.04	1.54±0.04	1.56±0.03	1.53±0.03	1.55±0.04	–

ADC measurements are presented as the mean ± standard deviation ($\times 10^{-3}$ mm^2/s). The P values were calculated as a comparison of the average ADC measurements between the SMS-DWI and CON-DWI. *, statistically significant (P<0.05). ADC, apparent diffusion coefficient; FLL, focal liver lesion; SMS, simultaneous multislice; DWI, diffusion-weighted imaging; CON, conventional; N, number of lesions; HCC, hepatocellular carcinoma; iCCA, intrahepatic cholangiocarcinoma; CHC, combined hepatocellular and cholangiocarcinoma; FNH, focal nodular hyperplasia; IMT, inflammatory myofibroblastic tumor; RN, regenerative nodule.

DWI ranged from 0.749 to 0.789, as shown in Table S4. This indicates consistent results between the radiologists, with no significant difference in DSC values between the SMS-DWI and CON-DWI sequences (P=0.101–0.582).

Discussion

Our study demonstrated that SMS-DWI with an acceleration factor of 2 can reduce the acquisition time by 37% while maintaining or slightly improving diagnostic image quality without significant artifacts. The consistency analysis showed moderate-to-excellent agreement for both intrareader and interreader reliability, indicating robust results.

SMS technology improves scanning efficiency, shortens acquisition time, expedites clinical examinations, and enhances patient comfort and cost-effectiveness. Previous studies have demonstrated how SMS-DWI can be used to reduce the scan time in various imaging examinations such as abdominal imaging (21,24,34), whole-body imaging (35,36), prostate imaging, and breast imaging (18,37,38), with comparable or improved image quality (16,17).

In SMS technology, multiple slices are simultaneously excited and correspondingly read out (15,39). By incorporating a blipped CAIPIRINHA technique, the reconstruction algorithm can separate the concurrently

acquired multiple slices (13,21), reducing repetition time (TR) or allowing broader coverage (36), thinner slice gaps (39,40), and more advanced diffusion protocols (23,41-43). Unlike parallel imaging, SMS technology does not involve reduced k-space sampling and is not susceptible to SNR loss, although SNR can decrease with significantly shortened TR (13). An acceleration factor of 2 is optimal for liver imaging, balancing scan time, image quality, and ADC measurements (15,23).

In liver imaging, SMS-DWI yields image quality comparable to or better than does CON-DWI (17,22,23,39,44,45). Obele *et al.* (22) found that in high b-value (b=800 s/mm^2) images, SMS-DWI achieved significantly higher overall image scores compared to CON-DWI. Tavakoli *et al.* (46) reported that respiratory-triggered SMS-DWI optimized image quality, provided better anatomical details, and reduced artifacts. Additionally, the high scanning efficiency of SMS-DWI can be used to enhance spatial resolution, thereby improving the detection rate of small lesions. Xu *et al.* (45) reported that SMS-DWI could detect more liver metastases (n=523) within the same scan time as compared to CON-DWI (n=348).

Currently, there is conflicting evidence regarding the impact of the SMS technique on liver DWI quantitative parameters. Some studies have found no significant difference in liver ADC values between SMS-DWI and CON-DWI, while others suggest that SMS-DWI increases liver ADC values (22,25). In our study, ADC values measured by CON-DWI exceeded those from SMS-DWI, especially in the HCC and iCCA groups. Similar findings were observed in other groups, but the differences were not statistically significant, likely due to the small sample size. Taron *et al.* also found that SMS-DWI resulted in lower ADC values in abdominal organs than did CON-DWI (16,21,24), with more significant differences at an acceleration factor of 3. They speculate that this might be due to incomplete recovery of the longitudinal magnetization vector (T1 saturation effect) affecting DWI and ADC signals. The partial volume effect of intravoxel fat signals can also affect ADC values (47). The ADC may be influenced by field strength, scanner type, the combination of b-values used, and different respiratory schemes (12,44,48). Absolute ADC values can differ among imaging protocols, complicating direct comparisons and potentially requiring different ADC thresholds for each sequence (49).

Notably, recent studies have indicated that T2 relaxation time significantly impacts ADC measurements, often more than does molecular diffusion (50-52). Wáng *et al.* found that short T2 times (<60 milliseconds) are negatively correlated with ADC values, while long T2 times (>80 milliseconds) are positively correlated (51). Liver tumors typically exhibit longer T2 times but lower ADC values, suggesting that T2 time has a more significant effect on DWI signals than does actual diffusion (52). Thus, in clinical applications, it is crucial to consider the impact of T2 time on ADC measurements to improve the accuracy of MRI diffusion imaging.

Different breathing schemes can affect absolute ADC values (16,26). Pei *et al.* found that breath-holding SMS-DWI provided comparable scan time reduction, image quality, good SNR, and the highest ADC repeatability at 3-T MRI as compared to CON-DWI and other breathing schemes (26). However, their study involved young, healthy volunteers with good breath-holding capability. Multiple studies have shown that SMS-DWI combined with respiratory triggering improves the image quality of the liver and kidneys compared to CON-DWI (16,20,46). Our study conducted DWI under free-breathing conditions without cardiac gating, potentially leading to motion artifacts and signal loss, especially in the left liver lobe (53). These artifacts degrade image quality, affecting lesion visibility and diagnostic accuracy. Incorporating motion compensation techniques such as advanced image registration or motion correction algorithms could address these challenges (53-55). Führes *et al.* (55) evaluated several postprocessing algorithms for improving flow-compensated liver diffusion image quality, finding the weighted averaging algorithm particularly effective in enhancing image quality and lesion conspicuity.

This study involved several limitations which should be acknowledged. First, the protocol was designed to be concise for routine clinical workflows, with only a single SMS acceleration setting being used (acceleration factor of 2). The potential of using higher acceleration factors remains unexplored and warrants further investigation, including in phantom model experiments. Second, the effects of other MRI sequences or different breathing schemes were not examined. We focused on applying SMS technology to DWI imaging in free-breathing mode, assessing its impact on scan time, image quality, and ADC measurements. Third, we only analyzed the average ADC measurements and did not include other relevant variables (such as maximum, minimum, or percentile) (56). Fourth, the sample size in some groups was relatively small, limiting further analysis. Fifth, subjective assessments of image quality and manual ROI drawings for quantitative

measurement could have introduced bias.

Future studies should be based on larger sample sizes to clarify the effects of SMS on quantitative measurements, image quality, and diagnostic performance with different acquisition parameters (scanners, breathing schemes, spatial resolutions, b-value combinations), diffusion models, postprocessing techniques, ROI delineation methods for lesions, and selection of ADC values (mean, minimum, etc.). This will help determine the optimal liver SMS settings for clinical use. Additionally, exploring other clinical applications of SMS technology beyond DWI sequences is recommended.

Conclusions

SMS-DWI achieved a 37% reduction in scan time compared to CON-DWI, maintaining similar overall image quality. This positions SMS-DWI as a viable alternative to CON-DWI within standard liver protocols; however, some caution should be used in interpreting its lower ADC values in diagnostic assessments.

Acknowledgments

Funding: This study was supported by grants from the National Natural Science Foundation of China (grant No. 82302161); the China Postdoctoral Science Foundation (grant No. 2023M732464); the Postdoctoral Fellowship Program of CPSF (grant No. GZB20230492); the Natural Science Foundation of Sichuan Province (grant No. 2024NSFSC1798); the Postdoctoral Research Fund of West China Hospital, Sichuan University (grant No. 2024HXBH161); the Hainan Province Clinical Medical Center; and the Postdoctoral Station Development Project of Sanya.

Footnote

Reporting Checklist: The authors have completed the GRRAS reporting checklist. Available at https://qims.amegroups.com/article/view/10.21037/qims-24-341/rc

Conflicts of Interest: All authors have completed the ICMJE uniform disclosure form (available at https://qims.amegroups.com/article/view/10.21037/qims-24-341/coif). B.S., Y.W., Z.Y., Ting Yang, S.Y., J.C., and H.T. received funding to support this research from the following sources: the National Natural Science Foundation of China (grant No. 82302161); the China Postdoctoral Science Foundation (grant No. 2023M732464), the Postdoctoral Fellowship Program of CPSF (grant No. GZB20230492); the Natural Science Foundation of Sichuan Province (grant No. 2024NSFSC1798); and the Postdoctoral Research Fund of West China Hospital, Sichuan University (grant No. 2024HXBH161). B.S. also received funding to support this research from the Hainan Province Clinical Medical Center and the Postdoctoral Station Development Project of Sanya. Ting Yin serves as a senior scientist for Research Collaboration in the MR Business Unit at Siemens Healthineers. The authors have no other conflicts of interest to declare.

Ethical Statement: The authors are accountable for all aspects of the work in ensuring that questions related to the accuracy or integrity of any part of the work are appropriately investigated and resolved. This prospective study was approved by the ethics committee of West China Hospital, Sichuan University (No. 2021[107]) and was conducted in accordance with the Declaration of Helsinki (as revised in 2013). Informed consent was obtained from 336 consecutive patients between February 2021 and March 2022.

References

1. Marrero JA, Ahn J, Rajender Reddy K; Americal College of Gastroenterology. ACG clinical guideline: the diagnosis and management of focal liver lesions. Am J Gastroenterol 2014;109:1328-47; quiz 1348.
2. Cannella R, Sartoris R, Grégory J, Garzelli L, Vilgrain V, Ronot M, Dioguardi Burgio M. Quantitative magnetic resonance imaging for focal liver lesions: bridging the gap between research and clinical practice. Br J Radiol 2021;94:20210220.
3. Gatti M, Maino C, Tore D, Carisio A, Darvizeh F, Tricarico E, Inchingolo R, Ippolito D, Faletti R. Benign focal liver lesions: The role of magnetic resonance

imaging. World J Hepatol 2022;14:923-43.
4. Surov A, Pech M, Omari J, Fischbach F, Damm R, Fischbach K, Powerski M, Relja B, Wienke A. Diffusion-Weighted Imaging Reflects Tumor Grading and Microvascular Invasion in Hepatocellular Carcinoma. Liver Cancer 2021;10:10-24.
5. Dreher C, Kuder TA, König F, Paech D, Tavakoli A, Laun FB, Flothow F, Gnirs R, Benkert T, Strecker R, Schlemmer HP, Bickelhaupt S. Advanced Diffusion-Weighted Abdominal Imaging: Qualitative and Quantitative Comparison of High and Ultra-High b-Values for Lesion Detection and Image Quality. Invest Radiol 2020;55:285-92.
6. Chernyak V, Fowler KJ, Kamaya A, Kielar AZ, Elsayes KM, Bashir MR, Kono Y, Do RK, Mitchell DG, Singal AG, Tang A, Sirlin CB. Liver Imaging Reporting and Data System (LI-RADS) Version 2018: Imaging of Hepatocellular Carcinoma in At-Risk Patients. Radiology 2018;289:816-30.
7. Drewes R, Pech M, Powerski M, Omari J, Heinze C, Damm R, Wienke A, Surov A. Apparent Diffusion Coefficient Can Predict Response to Chemotherapy of Liver Metastases in Colorectal Cancer. Acad Radiol 2021;28 Suppl 1:S73-80.
8. Niekamp A, Abdel-Wahab R, Kuban J, Odisio BC, Mahvash A, Hassan MM, Qayyum A, Kaseb A, Sheth RA. Baseline Apparent Diffusion Coefficient as a Predictor of Response to Liver-Directed Therapies in Hepatocellular Carcinoma. J Clin Med 2018;7:83.
9. Vandecaveye V, De Keyzer F, Verslype C, Op de Beeck K, Komuta M, Topal B, Roebben I, Bielen D, Roskams T, Nevens F, Dymarkowski S. Diffusion-weighted MRI provides additional value to conventional dynamic contrast-enhanced MRI for detection of hepatocellular carcinoma. Eur Radiol 2009;19:2456-66.
10. Guiu B, Cercueil JP. Liver diffusion-weighted MR imaging: the tower of Babel? Eur Radiol 2011;21:463-7.
11. Gultekin MA, Turk HM, Yurtsever I, Cesme DH, Seker M, Besiroglu M, Alkan A. Apparent Diffusion Coefficient Values for Neuroendocrine Liver Metastases. Acad Radiol 2021;28 Suppl 1:S81-6.
12. Taouli B, Koh DM. Diffusion-weighted MR imaging of the liver. Radiology 2010;254:47-66.
13. Setsompop K, Gagoski BA, Polimeni JR, Witzel T, Wedeen VJ, Wald LL. Blipped-controlled aliasing in parallel imaging for simultaneous multislice echo planar imaging with reduced g-factor penalty. Magn Reson Med 2012;67:1210-24.
14. Breuer FA, Blaimer M, Heidemann RM, Mueller MF, Griswold MA, Jakob PM. Controlled aliasing in parallel imaging results in higher acceleration (CAIPIRINHA) for multi-slice imaging. Magn Reson Med 2005;53:684-91.
15. Barth M, Breuer F, Koopmans PJ, Norris DG, Poser BA. Simultaneous multislice (SMS) imaging techniques. Magn Reson Med 2016;75:63-81.
16. Taron J, Martirosian P, Erb M, Kuestner T, Schwenzer NF, Schmidt H, Honndorf VS, Weiβ J, Notohamiprodjo M, Nikolaou K, Schraml C. Simultaneous multislice diffusion-weighted MRI of the liver: Analysis of different breathing schemes in comparison to standard sequences. J Magn Reson Imaging 2016;44:865-79.
17. Boss A, Barth B, Filli L, Kenkel D, Wurnig MC, Piccirelli M, Reiner CS. Simultaneous multi-slice echo planar diffusion weighted imaging of the liver and the pancreas: Optimization of signal-to-noise ratio and acquisition time and application to intravoxel incoherent motion analysis. Eur J Radiol 2016;85:1948-55.
18. Weiss J, Martirosian P, Taron J, Othman AE, Kuestner T, Erb M, Bedke J, Bamberg F, Nikolaou K, Notohamiprodjo M. Feasibility of accelerated simultaneous multislice diffusion-weighted MRI of the prostate. J Magn Reson Imaging 2017;46:1507-15.
19. Park JH, Seo N, Lim JS, Hahm J, Kim MJ. Feasibility of Simultaneous Multislice Acceleration Technique in Diffusion-Weighted Magnetic Resonance Imaging of the Rectum. Korean J Radiol 2020;21:77-87.
20. Tavakoli A, Krammer J, Attenberger UI, Budjan J, Stemmer A, Nickel D, Kannengiesser S, Morelli JN, Schoenberg SO, Riffel P. Simultaneous Multislice Diffusion-Weighted Imaging of the Kidneys at 3 T. Invest Radiol 2020;55:233-8.
21. Taron J, Martirosian P, Schwenzer NF, Erb M, Kuestner T, Weiß J, Othman A, Notohamiprodjo M, Nikolaou K, Schraml C. Scan time minimization in hepatic diffusion-weighted imaging: evaluation of the simultaneous multislice acceleration technique with different acceleration factors and gradient preparation schemes. MAGMA 2016;29:739-49.
22. Obele CC, Glielmi C, Ream J, Doshi A, Campbell N, Zhang HC, Babb J, Bhat H, Chandarana H. Simultaneous Multislice Accelerated Free-Breathing Diffusion-Weighted Imaging of the Liver at 3T. Abdom Imaging 2015;40:2323-30.
23. Xu H, Zhang N, Yang DW, Ren A, Ren H, Zhang Q, Zhu JX, Li GJ, Yang ZH. Feasibility study of simultaneous multislice diffusion kurtosis imaging with different

acceleration factors in the liver. BMC Med Imaging 2021;21:132.
24. Taron J, Martirosian P, Kuestner T, Schwenzer NF, Othman A, Weiß J, Notohamiprodjo M, Nikolaou K, Schraml C. Scan time reduction in diffusion-weighted imaging of the pancreas using a simultaneous multislice technique with different acceleration factors: How fast can we go? Eur Radiol 2018;28:1504-11.
25. Jang W, Song JS, Kwak HS, Hwang SB, Paek MY. Intra-individual comparison of conventional and simultaneous multislice-accelerated diffusion-weighted imaging in upper abdominal solid organs: value of ADC normalization using the spleen as a reference organ. Abdom Radiol (NY) 2019;44:1808-15.
26. Pei Y, Xie S, Li W, Peng X, Qin Q, Ye Q, Li M, Hu J, Hou J, Li G, Hu S. Evaluation of simultaneous-multislice diffusion-weighted imaging of liver at 3.0 T with different breathing schemes. Abdom Radiol (NY) 2020;45:3716-29.
27. Le Bihan D. Apparent diffusion coefficient and beyond: what diffusion MR imaging can tell us about tissue structure. Radiology 2013;268:318-22.
28. Norman G. Likert scales, levels of measurement and the "laws" of statistics. Adv Health Sci Educ Theory Pract 2010;15:625-32.
29. Goerner FL, Clarke GD. Measuring signal-to-noise ratio in partially parallel imaging MRI. Med Phys 2011;38:5049-57.
30. Liang X, Bi Z, Yang C, Sheng R, Xia X, Zhang Z, Dai Y, Zeng M. Free-Breathing Liver Magnetic Resonance Imaging With Respiratory Frequency-Modulated Continuous-Wave Radar-Trigger Technique: A Preliminary Study. Front Oncol 2022;12:918173.
31. Magnotta VA, Friedman L; FIRST BIRN. Measurement of Signal-to-Noise and Contrast-to-Noise in the fBIRN Multicenter Imaging Study. J Digit Imaging 2006;19:140-7.
32. Kundel HL, Polansky M. Measurement of observer agreement. Radiology 2003;228:303-8.
33. Yushkevich PA, Piven J, Hazlett HC, Smith RG, Ho S, Gee JC, Gerig G. User-guided 3D active contour segmentation of anatomical structures: significantly improved efficiency and reliability. Neuroimage 2006;31:1116-28.
34. Ciritsis A, Rossi C, Marcon M, Van VDP, Boss A. Accelerated diffusion-weighted imaging for lymph node assessment in the pelvis applying simultaneous multislice acquisition: A healthy volunteer study. Medicine (Baltimore) 2018;97:e11745.
35. Taron J, Schraml C, Pfannenberg C, Reimold M, Schwenzer N, Nikolaou K, Martirosian P, Seith F. Simultaneous multislice diffusion-weighted imaging in whole-body positron emission tomography/magnetic resonance imaging for multiparametric examination in oncological patients. Eur Radiol 2018;28:3372-83.
36. Krueger PC, Krämer M, Benkert T, Ertel S, Teichgräber U, Waginger M, Mentzel HJ, Glutig K. Whole-body diffusion magnetic resonance imaging with simultaneous multi-slice excitation in children and adolescents. Pediatr Radiol 2023;53:1485-96.
37. Ohlmeyer S, Laun FB, Palm T, Janka R, Weiland E, Uder M, Wenkel E. Simultaneous Multislice Echo Planar Imaging for Accelerated Diffusion-Weighted Imaging of Malignant and Benign Breast Lesions. Invest Radiol 2019;54:524-30.
38. Hu Y, Zhan C, Yang Z, Zhang X, Zhang H, Liu W, Xia L, Ai T. Accelerating acquisition of readout-segmented echo planar imaging with a simultaneous multi-slice (SMS) technique for diagnosing breast lesions. Eur Radiol 2021;31:2667-76.
39. Setsompop K, Cohen-Adad J, Gagoski BA, Raij T, Yendiki A, Keil B, Wedeen VJ, Wald LL. Improving diffusion MRI using simultaneous multi-slice echo planar imaging. Neuroimage 2012;63:569-80.
40. Machida Y, Nomura K, Shimauchi A, Kato Y, Nagatsuka M, Fukuma E. Diffusion-weighted imaging with simultaneous multi-slice echo-planar technique for the diagnosis of breast magnetic resonance imaging. Jpn J Radiol 2020;38:358-64.
41. Wang F, Wu C, Sun C, Liu D, Sun Y, Wang Q, Jin Z. Simultaneous Multislice Accelerated Diffusion Tensor Imaging of Thigh Muscles in Myositis. AJR Am J Roentgenol 2018;211:861-6.
42. Wáng YXJ, Sabarudin A. Underestimation of liver hemangioma perfusion fraction by standard intravoxel incoherent motion diffusion magnetic resonance imaging. Quant Imaging Med Surg 2024;14:2128-35.
43. Wáng YXJ. Observed paradoxical perfusion fraction elevation in steatotic liver: An example of intravoxel incoherent motion modeling of the perfusion component constrained by the diffusion component. NMR Biomed 2021;34:e4488.
44. Chen X, Qin L, Pan D, Huang Y, Yan L, Wang G, Liu Y, Liang C, Liu Z. Liver diffusion-weighted MR imaging: reproducibility comparison of ADC measurements obtained with multiple breath-hold, free-breathing, respiratory-triggered, and navigator-triggered techniques. Radiology 2014;271:113-25.

45. Xu J, Cheng YJ, Wang ST, Wang X, Jin ZY, Qian TY, Zhu JX, Nickel MD, Xue HD. Simultaneous multi-slice accelerated diffusion-weighted imaging with higher spatial resolution for patients with liver metastases from neuroendocrine tumours. Clin Radiol 2021;76:81.e11-9.
46. Tavakoli A, Attenberger UI, Budjan J, Stemmer A, Nickel D, Kannengiesser S, Morelli JN, Schoenberg SO, Riffel P. Improved Liver Diffusion-Weighted Imaging at 3 T Using Respiratory Triggering in Combination With Simultaneous Multislice Acceleration. Invest Radiol 2019;54:744-51.
47. Zeilinger MG, Lell M, Baltzer PA, Dörfler A, Uder M, Dietzel M. Impact of post-processing methods on apparent diffusion coefficient values. Eur Radiol 2017;27:946-55.
48. Dale BM, Braithwaite AC, Boll DT, Merkle EM. Field strength and diffusion encoding technique affect the apparent diffusion coefficient measurements in diffusion-weighted imaging of the abdomen. Invest Radiol 2010;45:104-8.
49. Sasaki M, Yamada K, Watanabe Y, Matsui M, Ida M, Fujiwara S, Shibata E; Acute Stroke Imaging Standardization Group-Japan (ASIST-Japan) Investigators. Variability in absolute apparent diffusion coefficient values across different platforms may be substantial: a multivendor, multi-institutional comparison study. Radiology 2008;249:624-30.
50. Wáng YXJ, Zhao KX, Ma FZ, Xiao BH. The contribution of T2 relaxation time to MRI-derived apparent diffusion coefficient (ADC) quantification and its potential clinical implications. Quant Imaging Med Surg 2023;13:7410-6.
51. Wáng YXJ, Ma FZ. A tri-phasic relationship between T2 relaxation time and magnetic resonance imaging (MRI)-derived apparent diffusion coefficient (ADC). Quant Imaging Med Surg 2023;13:8873-80.
52. Li XM, Yao DQ, Quan XY, Li M, Chen W, Wáng YXJ. Perfusion of hepatocellular carcinomas measured by diffusion-derived vessel density biomarker: Higher hepatocellular carcinoma perfusion than earlier intravoxel incoherent motion reports. NMR Biomed 2024;37:e5125.
53. Liau J, Lee J, Schroeder ME, Sirlin CB, Bydder M. Cardiac motion in diffusion-weighted MRI of the liver: artifact and a method of correction. J Magn Reson Imaging 2012;35:318-27.
54. Chang LC, Walker L, Pierpaoli C. Informed RESTORE: A method for robust estimation of diffusion tensor from low redundancy datasets in the presence of physiological noise artifacts. Magn Reson Med 2012;68:1654-63.
55. Führes T, Saake M, Lorenz J, Seuss H, Stemmer A, Benkert T, Uder M, Laun FB. Reduction of the cardiac pulsation artifact and improvement of lesion conspicuity in flow-compensated diffusion images in the liver-A quantitative evaluation of postprocessing algorithms. Magn Reson Med 2023;89:423-39.
56. Bickel H, Pinker K, Polanec S, Magometschnigg H, Wengert G, Spick C, Bogner W, Bago-Horvath Z, Helbich TH, Baltzer P. Diffusion-weighted imaging of breast lesions: Region-of-interest placement and different ADC parameters influence apparent diffusion coefficient values. Eur Radiol 2017;27:1883-92.

Cite this article as: Wu Y, Ye Z, Yang T, Yao S, Chen J, Yin T, Tang H, Song B. Simultaneous multislice echo-planar diffusion-weighted imaging (DWI) in patients with focal liver lesions: a comparative study with conventional DWI. Quant Imaging Med Surg 2024;14(9):6684-6697. doi: 10.21037/qims-24-341

